Received 4 November 2022; revised 28 December 2022; accepted 2 January 2023. Date of publication 6 January 2023;
date of current version 21 February 2023. The review of this article was arranged by Editor G. I. Ng.

Digital Object Identifier 10.1109/JEDS.2023.3234695

InAlN/GaN HEMT With n$^+$GaN Contact Ledge Structure for Millimeter-Wave Low Voltage Applications

CAN GONG[1], MINHAN MI[1], YUWEI ZHOU[2], PENGFEI WANG[1], YILIN CHEN[2], JIELONG LIU[2], YUTONG HAN[1], SIRUI AN[1], SIYIN GUO[1], MENG ZHANG[1], QING ZHU[1], MEI YANG[1], XIAOHUA MA[1] (Member, IEEE), AND YUE HAO[1] (Senior Member, IEEE)

1 State Key Discipline Laboratory of Wide Band-Gap Semiconductor Technology, School of Microelectronics, Xidian University, Xi'an 710071, China
2 School of Advanced Materials and Nanotechnology, Xidian University, Xi'an 710071, China

CORRESPONDING AUTHOR: M. MI (e-mail: miminhan@qq.com)

This work was supported in part by the National Key Research and Development Project of China under Grant 2021YFB3602404; in part by the National Natural Science Foundation of China under Grant 61904135 and Grant 62234009; in part by the Key Research and Development Program of Guangzhou under Grant 202103020002; in part by Wuhu and Xidian University Special Fund for Industry–University–Research Cooperation under Grant XWYCXY-012021014-HT; in part by the Fundamental Research Funds for the Central Universities under Grant XJS221110; and in part by the Natural Science Foundation of Shaanxi, China, under Grant 2022JM-377.

ABSTRACT In this work, high performance InAlN/GaN HEMT based on the n$^+$GaN regrown ohmic contact with n$^+$GaN contact ledge structure is proposed. The regrown ohmic contact of InAlN/GaN HEMT is formed by MBE n$^+$GaN regrowth and self-stopping etching, which makes the total ohmic contact resistance between the 2DEG channel and the ohmic metal decrease to 0.12 Ω·mm and forms n$^+$GaN contact ledge structure. Owing to the n$^+$GaN contact ledge on the InAlN barrier, with the increasing of drain-source voltage (V_{DS}), an additional current path comes into being between the n$^+$GaN contact ledge on the InAlN barrier and the 2DEG channel, which can "shorten" the device effective drain-source distance, thus further reducing the parasitic resistance. Compared with regrown InAlN/GaN HEMT without n$^+$GaN contact ledge structure, the peak transconductance ($G_{m.max}$) of regrown InAlN/GaN HEMT with n$^+$GaN contact ledge structure increases from 747 mS/mm to 874 mS/mm, and the saturation current density ($I_{D.max}$) increases from 2.6 A/mm to 2.9 A/mm. Besides, the self-stopping etching on the access region does not induce extra defects, and negligible current collapse is obtained. As the results of low parasitic resistance, high output current density, low knee voltage and negligible current collapse, power-added-efficiency (PAE) of 44% together with output power density (P_{out}) of 2.5 W/mm is achieved at 30 GHz and V_{DS} of 10 V, which indicates regrown InAlN/GaN HEMT with n$^+$GaN contact ledge structure has great potential for millimeter-wave low voltage applications. Additionally, the transfer and schottky gate characteristics show negligible degradation after OFF/ON-state electrical stress tests.

INDEX TERMS InAlN/GaN HEMT, n$^+$GaN contact ledge, low voltage *RF* applications.

I. INTRODUCTION

Benefitting from the large critical electric field (∼3.3 MV), the high electron saturation drift velocity (∼2.5×10^7 cm/s), and the high two-dimensional electron gas (2DEG) density (∼2×10^{13} cm^{-2}), GaN-based high electron mobility transistor (HEMT) shows great potential for high power and high frequency applications [1]. However, with the development of the 5G wireless communication technologies, future mobile terminals need to operate at millimeter-wave frequency with a lower supply voltage. For example, in order to achieve as long as possible standby time, mobile phones, laptops, and GPS locators are required to ensure high efficiency and low power consumption while powered by battery packs. Compared with Si-based and GaAs-based RF devices, GaN HEMTs have advantages in power-added-efficiency (PAE) and output power density (P_{out}) at low supply voltage [2], [3], exhibiting great consumption space of low voltage GaN RF applications.

In order to achieve high PAE and large P_{out} for low voltage RF devices, it is important to increase the maximum output current density ($I_{D.max}$) and reduce the knee voltage (V_{knee}) [4], [5], [6]. Therefore, reducing the parasitic resistance, including access resistance and ohmic contact resistance, is a key technology. The access resistance is determined by the drain-source distance and the sheet resistance of the heterostructure. In order to reduce the access resistance, self-aligned gate technology can be used to scale down the drain-source distance and strongly polarized heterojunction can be utilized to reduce the sheet resistance of the 2DEG channel [7], [8]. To reduce ohmic contact resistance, at present, n^+GaN regrown ohmic contact technology is commonly used [9], [10]. Furthermore, TiN-based and n^+GaN cap contact ledge structures have been used to provide a current path between the contact ledge and the 2DEG channel to further increase the maximum output current density [11], [12]. However, annealing process needs to be introduced to form the TiN-based ledge, which leads to worse surface morphology and causes the ohmic metals edge to expand outward [13], which makes the minimum drain-source spacing can only scaled to 3μm, and it is difficult to further reduce the drain-source spacing to submicron dimension. For previous n^+GaN cap contact ledge structure device in [12], n^+GaN cap did not interact with the 2DEG channel. The ohmic contact resistance still needed to be reduced. Besides, it was difficult to control the etching time accurately and make the etching stop on the surface of the barrier by Cl-based etching. Therefore, if self-stopping etching technology was used, it is advantageous for non-alloyed n^+GaN regrown ohmic contact combined with the n^+GaN contact ledge structure to scale down the access dimension and reduce the parasitic resistance.

Based on the above, regrown InAlN/GaN HEMT with n^+GaN contact ledge structure has been fabricated by regrown ohmic contact and self-stopping etching technology in this work, and its ohmic contact resistance reaches 0.12 Ω·mm. An additional current path between n^+GaN regrown contact ledge and 2DEG channel is formed, which "redefines" the device drain-source distance thus reducing the effective drain-source spacing. Although this structure has been reported in previous work [14], the GaN cap layer is inevitably etched during the self-stopping etching process, resulting in output current degradation and large gate leakage current. This work not only optimizes the device structure to 10 nm InAlN barrier replacing the previous InAlN layer combined with GaN cap layer to solve the above problems, but also evaluates the long-term reliability of this newly proposed structure. Therefore, with the assistance of optimized barrier structure and n^+GaN regrown contact ledge, the regrown InAlN/GaN HEMT could obtain $I_{D.max}$ of 2.9 A/mm. Although self-stopping etching is performed on the access region, current collapse of the device can be ignored under low voltage operating conditions. The device with the gate length of 150 nm achieves f_T/f_{MAX} of 93 GHz/142 GHz. Notably, due to the lower parasitic resistance and larger output current density, output power density (P_{out}) of 2.5 W/mm and PAE of 44% are realized at 30 GHz and V_{DS} of 10 V for regrown InAlN/GaN HEMT with n^+GaN contact ledge structure. After OFF-state and ON-state electrical stress measurements, the drain current and the schottky gate current of the proposed device show negligible degradation, indicating that the regrown HEMT with n^+GaN contact ledge structure has decent stability.

II. DEVICE FABRICATION PROCESS

Device fabrication process of regrown InAlN/GaN HEMT with contact ledge structure is demonstrated in Fig. 1. As shown in the Fig. 1(a), the epi-layers of InAlN/GaN heterojunction were grown by metal-organic-chemical vapor deposition (MOCVD) on SiC substrate, containing 10 nm $In_{0.17}Al_{0.83}N$ barrier and GaN buffer. The carrier density of 2.4×10^{13} cm^{-2} and mobility of 1638 $cm^2/V\cdot s$ were measured by room temperature Hall measurement.

The device fabrication process began with the definition of the regrowth region via stepper lithography. Next, BCl_3/Cl_2 ICP plasma dry etching was used to form a steep etching side wall and wet treatments were performed to remove surface impurities to decrease the interface resistance between the regrown n^+GaN and 2DEG channel. The drain-source distance (L_{DS}) was 600 nm, defined by the spacing of the two etching wells as shown in Fig. 1(b). Then, 80 nm n^+GaN with heavily doped Si (> 2×10^{20} cm^{-3}) was regrown on the whole wafer by MBE. After that, device isolation was achieved by boron ion implantation. Subsequently, partial n^+GaN on the access region was defined by Electron-Beam-Lithography (EBL) and removed via BCl_3/SF_6 ICP plasma dry etching to form the contact ledge. Previous work reported that BCl_3/SF_6 mixed gas plasma dry etching can etch the regrown n^+GaN and spontaneously stop on the Al-containing barrier, while ensures the smoothness of the barrier surface. When the SF_6 plasma reaches the InAlN barrier surface, the fluorine ion reacts with the Al atoms and forms a thin AlF_3 etching stop layer [15]. After BCl_3/SF_6 ICP plasma self-stopping etching, the byproduct was removed by ammonia water treatment at 55°C for 10 mins. As shown in Fig. 1(e), n^+GaN contact ledges overhung on the InAlN barrier from both drain and source etching wells to gate side. Afterwards, the nonalloyed Ti/Al/Ni/Au ohmic contact metals of 20/160/55/45 nm were deposited by electron beam evaporation and a 120 nm SiN layer was deposited by PECVD to provide a surface passivation. Then, 150 nm gate foot was defined by EBL and removed SiN by CF_4 plasma dry etching. Finally, gate head was defined by stepper lithography and Ni/Au gate metals were deposited by electron beam evaporation.

As shown in Fig. 1(j), regrown InAlN/GaN HEMT with n^+GaN contact ledge structure had been fabricated. The distance between the drain etching well and the source etching well was defined as drain-source spacing (L_{DS}), which was shrunk to 600 nm, as well as the gate width was 2×50 μm. T-gate was in the middle of the drain and source region. The

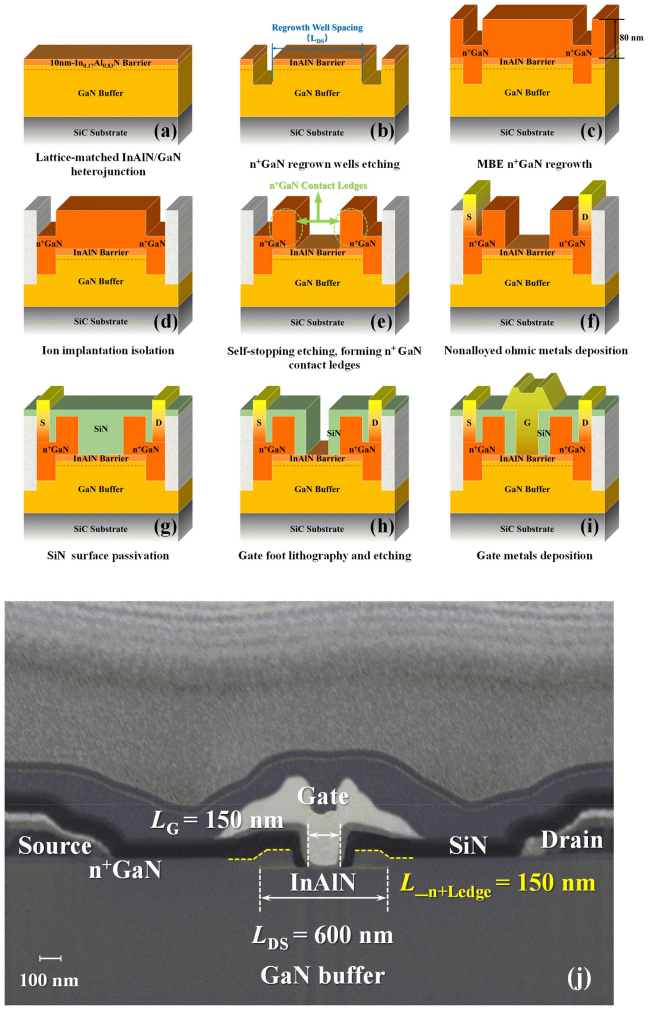

FIGURE 1. (a)~(i) The fabrication process flow of regrown InAlN/GaN HEMT with n+GaN contact ledge structure. (j) SEM characterization of fabricated InAlN/GaN HEMT with n+GaN contact ledge structure.

T-gate length (L_G) was 150 nm, while the n+GaN contact ledge length ($L_{\_n+Ledge}$) on each side was also 150 nm.

III. DEVICE CHARACTERISTICS AND DISCUSSION

A. TLM MEASUREMENT AND DISCUSSION

As shown in Fig. 2(a) and (b), in order to characterize ohmic contact resistance, two kinds of TLM patterns are designed [16]. TLM results are shown in Fig. 2(c). By measuring TLM1, the resistance R_1 between ohmic metal and n+GaN is 0.03 Ω·mm, as well as the sheet resistance of n+GaN (R_{SH_n+GaN}) is 47 Ω/□. According to TLM2 measurement, 2DEG channel sheet resistance (R_{SH_2DEG}) is 162 Ω/□, and the total ohmic contact resistance R_C of the device is 0.12 Ω·mm, including the resistance between ohmic metal and n+GaN (R_1 of 0.03 Ω·mm), resistance of n+GaN access region (R_2 of 0.035 Ω·mm) calculated by multiplying R_{SH_n+GaN} by the distance from the ohmic metal to the etching side wall, and the interface resistance between n+GaN and 2DEG channel (R_3 of 0.055 Ω·mm).

Fig. 2(d) shows that the TLM pattern with n+GaN regrown contact ledge structure has a higher maximum output current density than the pattern without n+GaN regrown contact ledge, both with the same drain-source distance of 3 μm, however, the on-resistance of the two devices is basically the same. This phenomenon could be explained by Fig. 2(e) based on Silvaco TCAD simulation. With the assistance of Silvaco TCAD simulation, the energy band between source n+GaN regrown contact ledge and 2DEG channel are shown in Fig. 2(f) to further explain the phenomenon mentioned above. As shown in Fig. 2(f), at lower drain-source voltage (such as 0~1 V), the InAlN barrier width between source n+GaN contact ledge and 2DEG channel are still large, which is difficult for electrons to transfer from source n+GaN contact ledge to 2DEG channel in source region, so that only current Path 1 has been turned on. As drain voltage increases, the barrier width and height between source n+GaN contact ledge and 2DEG channel become thinner and lower, and electrons could easily transfer from source n+GaN contact ledge to 2DEG channel through tunneling or thermal electron emission, so that the current Path 2 has been gradually turned on. When the device is biased at a higher drain-source voltage (such as V_{DS} = 10 V), both the current Path 1 and Path 2 contribute to the drain current increment, corresponding to the reduction of drain-source effective spacing.

B. DC CHARACTERISTICS

The InAlN/GaN HEMT adopting regrown ohmic contact without contact ledge structure has been fabricated as well. The device has the same size and adopts the n+GaN regrowth technology, but there is only no n+GaN contact ledge structure. The schematic figures of the regrown InAlN/GaN HEMT with and without n+GaN contact ledge structure were shown in Fig. 3(a) and (b).

The DC characteristics of the regrown InAlN/GaN HEMT with and without n+GaN contact ledge structure were measured by Keithley 4200 semiconductor parameter analyzer. The transfer characteristics of the two regrown InAlN/GaN HEMTs were measured at V_{DS} of 10 V, as shown in Fig. 4(a). Benefitting from the n+GaN contact ledge structure providing an additional current path and scaling down the effective drain-source spacing, the peak extrinsic transconductance ($G_{m.max}$) of the regrown HEMT with n+GaN contact ledge is 127 mS/mm larger than the one without n+GaN contact ledge, reaching 874 mS/mm.

Fig. 4(b) shows the output characteristics with the maximum gate voltage ($V_{GS.max}$) of 2 V, with the assistance of n+GaN contact ledge structure, the maximum output current density ($I_{D.max}$) of the HEMT is 2.9 A/mm, which is 246 mA/mm larger than the regrown HEMT without n+GaN contact ledge structure. Both regrown n+GaN ohmic contact and contact ledge structure are responsible for the improved DC performance.

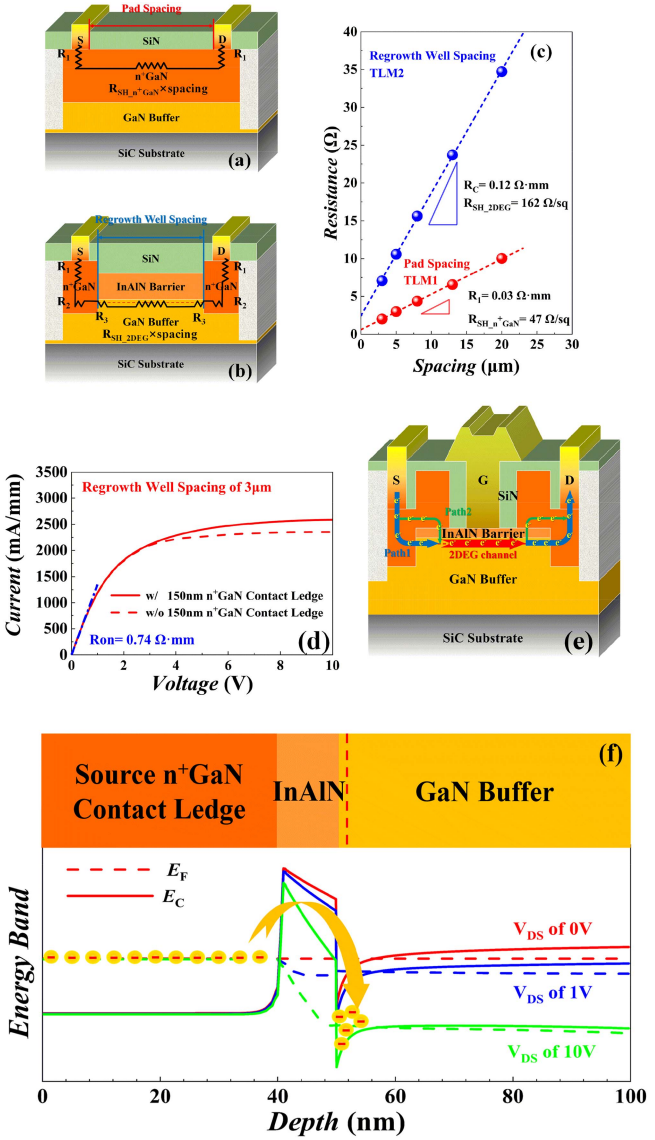

FIGURE 2. (a) TLM pattern on regrown n+GaN. (b) TLM pattern on InAlN/GaN heterojunction for n+GaN regrown device without contact ledge structure. (c) TLM measurement results for regrown device without n+GaN contact ledge structure. (d) Influence of n+GaN contact ledge structure by current measurement on TLM pattern with 3 μm drain-source distance. (e) Schematic diagram of regrown InAlN/GaN device with n+GaN contact ledge structure forming a second current path. (f) Energy band simulation diagrams of source n+GaN contact ledge region at three typical bias voltages.

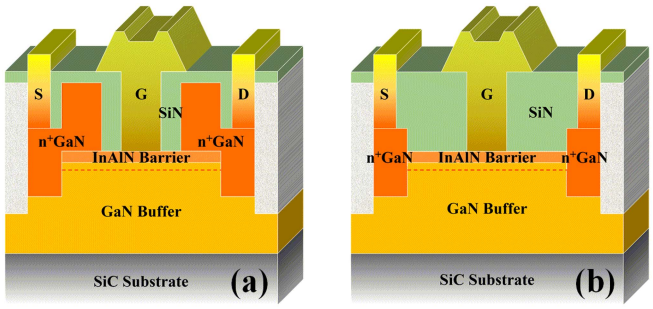

FIGURE 3. (a) The schematic figure of the regrown InAlN/GaN HEMT with and (b) without n+GaN contact ledge structure.

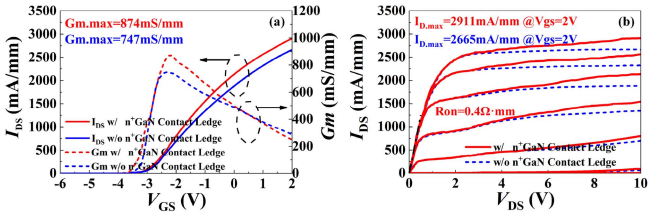

FIGURE 4. Comparison of (a) Transfer characteristics and (b) Output characteristics between regrown InAlN/GaN HEMT with and without n+GaN contact ledge structure.

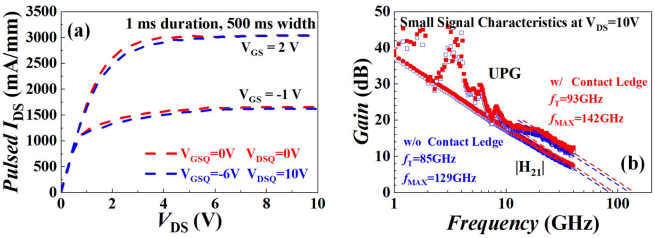

FIGURE 5. (a) Pulsed I-V characteristics and (b) Small signal characteristics of regrown InAlN/GaN HEMT with and without n+GaN contact ledge structure.

C. PULSED I-V & SMALL SIGNAL CHARACTERISTICS

As shown in Fig. 5(a), the pulsed I-V characteristics were measured with quiescent bias points of (V_{GSQ}, V_{DSQ} = 0 V, 0 V) and (V_{GSQ}, V_{DSQ} = −6 V, 10 V). The pulse period was 1 ms and the pulse width was 500 ns. The current collapse is only 2%, and the negligible current collapse indicates that the self-stopping etching on the access region does not induce extra damage.

The Agilent 8363B vector network analyzer was used to measure the small signal characteristics. Benefitting from the n+GaN contact ledge providing an additional current path and reducing the effective drain-source spacing, the access resistance is reduced. Therefore, the regrown InAlN/GaN HEMT with n+GaN contact ledge has larger f_T and f_{MAX} than regrown HEMT without n+GaN contact ledge. As shown in Fig. 5(b), by extrapolating the short circuit current gain ($|H_{21}|$) and the Mason's unilateral gain (UPG) curves using −20 dB/decade slopes, f_T and f_{MAX} of the regrown InAlN/GaN HEMT with n+GaN contact ledge at V_{DS} of 10 V are 93 GHz and 142 GHz, respectively. The small-signal performance can fully meet the requirement of millimeter-wave low voltage applications.

D. RF POWER CHARACTERISTICS

The on-wafer load-pull system was used to measure the RF power characteristics of the regrown HEMTs with and without n+GaN contact ledge at 30 GHz, and both input and output impedances of the devices were tuned to optimize the power-added-efficiency (PAE). Two kinds of the InAlN/GaN HEMTs were both biased at V_{DS} of 10 V and I_{DQ} of 100 mA/mm. What's more, with the assistance of the n+GaN

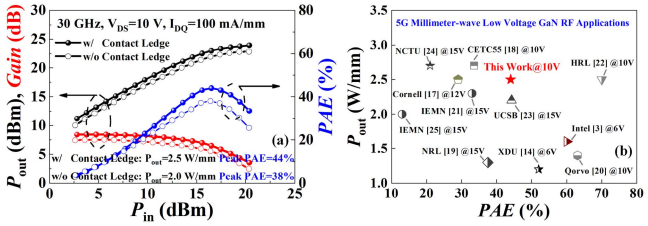

FIGURE 6. **(a) Comparison on the RF power characteristics between regrown InAlN/GaN HEMT with and without n+GaN contact ledge structure. (b) Comparison of P_{out} and PAE between GaN HEMTs and regrown InAlN/GaN HEMT with n+GaN contact ledge structure in the Ka band for low voltage application (5∼15 V).**

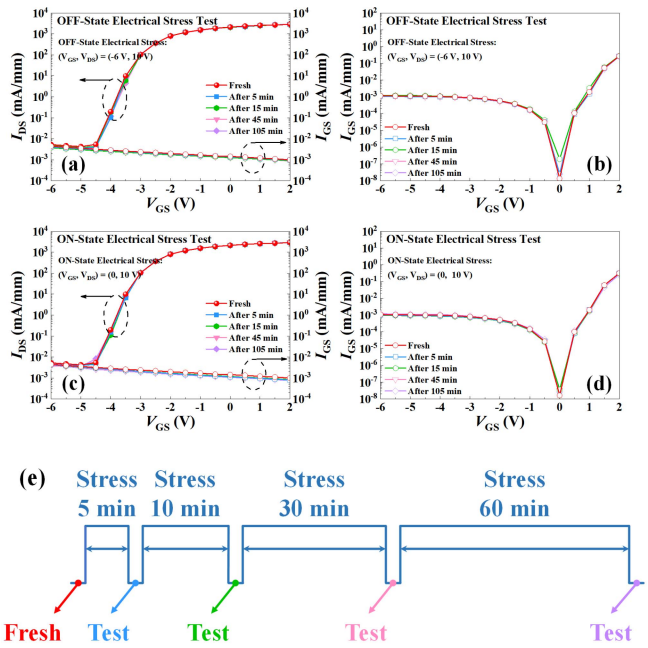

FIGURE 7. **Comparison of (a) transfer characteristics and (b) schottky gate characteristics before and after OFF-state electrical stress test. Comparison of (c) transfer characteristics and (d) schottky gate characteristics before and after ON-state electrical stress test. (e) The schematic of OFF/ON-state electrical stress measurements of the regrown device with n+GaN contact ledge structure.**

contact ledge reducing the effective drain-source spacing, the regrown InAlN/GaN HEMT with n+GaN contact ledge structure has the lower parasitic resistance and larger output current density, which makes the regrown InAlN/GaN HEMT with n+GaN contact ledge structure deliver a higher peak PAE and larger P_{out}. The regrown InAlN/GaN HEMT with n+GaN contact ledge structure delivers a PAE of 44% with a P_{out} of 2.5 W/mm, as shown in Fig. 6(a).

Within the Ka band, the regrown InAlN/GaN HEMT with n+GaN contact ledge structure has decent power performance by comparing the power characteristics of GaN HEMTs under similar low voltage bias, as shown in Fig. 6(b), which indicates great advantage of regrown InAlN/GaN HEMT with n+GaN contact ledge structure for millimeter-wave low voltage terminal applications. However, the maximum applicable V_{DS} is reduced due to the shorter effective gate-drain spacing. But considering that the device works for low voltage terminal applications, the operating voltage of the device is usually 5∼15 V, so that the reduction of the applicable V_{DS} would be tolerated. In our subsequent work, the reduction of the maximum applicable V_{DS} caused by the shorter effective gate-drain spacing of the device will be considered and handled. The n+GaN contact ledge on the drain side will be removed to increase the applicable voltage range of the device.

E. ELECTRICAL STRESS RELIABILITY

Reliability is critical for RF devices. Therefore, the electrical stress reliability of this newly proposed device with n+GaN contact ledge structure formed by self-stopping etching was evaluated. As shown in Fig. 7, the OFF-state and ON-state electrical stress tests have been adopted to assess the reliability of the regrown InAlN/GaN HEMT with n+GaN contact ledge structure. The OFF-state electrical stress condition was $V_{GS} = -6$ V and $V_{DS} = 10$ V, and the ON-state electrical stress condition was $V_{GS} = 0$ V and $V_{DS} = 10$ V. The threshold voltage, drain current, and schottky gate current have negligible change after OFF-state and ON-state electrical stress measurements. It can be seen that the regrown HEMT with n+GaN contact ledge structure has decent stability by electrical stress evaluation.

IV. CONCLUSION

In conclusion, high performance regrown InAlN/GaN HEMT with n+GaN contact ledge structure for low voltage application has been fabricated. The fabricated device has low on-resistance and ohmic contact resistance. In particular, attribute to the n+GaN contact ledges shortening the effective drain-source distance, the $G_{m.max}$ of the device reaches 874 mS/mm, $I_{D.max}$ reaches 2.9 A/mm. Ignorable current collapse indicates that no excessive etching damage was introduced on the self-stopping etching region. It is worth noting that regrown InAlN/GaN HEMT with n+GaN contact ledge structure exhibits PAE of 44% and P_{out} of 2.5 W/mm at 30 GHz and V_{DS} of 10 V, indicating great potential of regrown InAlN/GaN HEMT with n+GaN contact ledge structure for 5G millimeter-wave band low voltage applications. Besides, by OFF/ON-state electrical stress measurements, the regrown HEMT with n+GaN contact ledge can be proved to have good reliability.

REFERENCES

[1] U. K. Mishra, L. Shen, T. E. Kazior, and Y.-F. Wu, "GaN-based RF power devices and amplifiers," *Proc. IEEE*, vol. 96, no. 2, pp. 287–305, Feb. 2008, doi: 10.1109/JPROC.2007.911060.

[2] H. W. Then et al., "High-performance low-leakage enhancement-mode high-K dielectric GaN MOSHEMTs for energy-efficient, compact voltage regulators and RF power amplifiers for low-power mobile SoCs," in *Proc. Symp. VLSI Technol.*, 2015, pp. T202–T203, doi: 10.1109/VLSIT.2015.7223674.

[3] H. W. Then et al., "Advanced scaling of enhancement mode high-K gallium nitride-on-300mm-Si (111) transistor and 3D layer transfer GaN-silicon finfet CMOS integration," in *IEEE Int. Electron Devices Meeting Tech. Dig.*, 2021, pp. 11.1.1–11.1.4, doi: 10.1109/IEDM19574.2021.9720710.

[4] P. Saunier et al., "InAlN barrier scaled devices for very high f_T and for low-voltage RF applications," *IEEE Trans. Electron Devices*, vol. 60, no. 10, pp. 3099–3104, Oct. 2013, doi: 10.1109/TED.2013.2277772.

[5] Z. Zheng et al., "GaN HEMT with convergent channel for low intrinsic knee voltage," *IEEE Electron Device Lett.*, vol. 41, no. 9, pp. 1304–1307, Sep. 2020, doi: 10.1109/LED.2020.3010810.

[6] Y. Zhou et al., "Analysis of low voltage RF power capability on AlGaN/GaN and InAlN/GaN HEMTs for terminal applications,"*IEEE J. Electron Devices Soc.*, vol. 9, pp. 756–762, 2021, doi: 10.1109/JEDS.2021.3103847.

[7] K. Shinohara et al., "Scaling of GaN HEMTs and Schottky diodes for submillimeter-wave MMIC applications," *IEEE Trans. Electron Devices*, vol. 60, no. 10, pp. 2982–2996, Oct. 2013, doi: 10.1109/TED.2013.2268160.

[8] Y. Tang et al., "Ultrahigh-speed GaN high-electron-mobility transistors with f_T/f_{max} of 454/444 GHz," *IEEE Electron Device Lett.*, vol. 36, no. 6, pp. 549–551, Jun. 2015, doi: 10.1109/LED.2015.2421311.

[9] F. A. Faria et al., "Ultra-low resistance ohmic contacts to GaN with high Si doping concentrations grown by molecular beam epitaxy," *IEEE Appl. Phys. Lett.*, vol. 101, Jul. 2012, Art. no. 32109, doi: 10.1063/1.4738768.

[10] A. Hickman et al., "First RF power operation of AlN/GaN/AlN HEMTs with >3 A/mm and 3 W/mm at 10 GHz," *IEEE J. Electron Devices Soc.*, vol. 9, pp. 121–124, 2021, doi: 10.1109/JEDS.2020.3042050.

[11] L. Yang et al., "Enhanced gm and fT with high Johnson''s figure-of-merit in thin barrier AlGaN/GaN HEMTs by TiN-based source contact ledge," *IEEE Electron Device Lett.*, vol. 38, no. 11, pp. 1563–1566, Nov. 2017, doi: 10.1109/LED.2017.2757523.

[12] J. S. Moon et al., "55% PAE and high power Ka-band GaN HEMTs with linearized transconductance via n$^+$GaN source contact ledge," *IEEE Electron Device Lett.*, vol. 29, no. 8, pp. 834–837, Aug. 2008, doi: 10.1109/LED.2008.2000792.

[13] R. M. Gong et al., "Analysis of surface roughness in Ti/Al/Ni/Au ohmic contact to AlGaN/GaN high electron mobility transistors,"*IEEE Appl. Phys. Lett.*, vol. 97, Aug. 2010, Art. no. 62115, doi: 10.1063/1.3479928.

[14] Y. Zhou et al., "High performance millimeter-wave InAlN/GaN HEMT for low voltage RF applications via regrown ohmic contact with contact ledge structure," *IEEE Appl. Phys. Lett.*, vol. 120, Feb. 2022, Art. no. 62104, doi: 10.1063/5.0079359.

[15] Y.-C. Chang, Y.-L. Ho, T.-Y. Huang, D.-W. Huang, and C.-H. Wu, "Investigation of normally-off p-GaN/AlGaN/GaN HEMTs using a self-terminating etching technique with multi-finger architecture modulation for high power application," *Micromachines*, vol. 12, no. 4, p. 432, Apr. 2021, doi: 10.3390/mi12040432.

[16] J. Guo et al., "MBE-regrown ohmics in InAlN HEMTs with a regrowth interface resistance of 0.05 Ω·mm," *IEEE Electron Device Lett.*, vol. 33, no. 4, pp. 525–527, Apr. 2012, doi: 10.1109/LED.2012.2186116.

[17] A. Hickman et al., "Large signal response of AlN/GaN/AlN HEMTs at 30 GHz," in *Proc. Device Res. Conf. (DRC)*, 2021, pp. 1–2, doi: 10.1109/DRC52342.2021.9467196.

[18] W. Wang et al., "Improvement of power performance of GaN HEMT by using quaternary InAlGaN barrier," *IEEE J. Electron Devices Soc.*, vol. 6, pp. 360–364, 2018, doi: 10.1109/JEDS.2018.2807185.

[19] B. P. Downey, D. J. Meyer, D. S. Katzer, J. A. Roussos, M. Pan, and X. Gao, "SiN_x/InAlN/AlN/GaN MIS-HEMTs with 10.8 THz·V Johnson figure of merit," *IEEE Electron Device Lett.*, vol. 35, no. 5, pp. 527–529, May 2014, doi: 10.1109/LED.2014.2313023.

[20] Y. Cao et al., "Qorvo's emerging GaN technologies for mmWave applications," in *IEEE/MTT-S Int. Microw. Symp. Tech. Dig.*, 2020, pp. 570–572, doi: 10.1109/IMS30576.2020.9223913.

[21] F. Medjdoub, E. Okada, B. Grimbert, M. Zegaoui, D. Ducatteau, and N. Rolland, "Towards millimeter-wave high PAE high power using ultrathin Al-rich barrier GaN devices," in *Proc. Asia–Pacific Microw. Conf.*, 2014, pp. 777–779.

[22] J.-S. Moon et al., "Power scaling of graded-channel GaN HEMTs with mini-field-plate T-gate and 156 GHz f_T," *IEEE Electron Device Lett.*, vol. 42, no. 6, pp. 796–799, Jun. 2021, doi: 10.1109/LED.2021.3075926.

[23] M. Higashiwaki, Y. Pei, R. Chu, and U. K. Mishra, "Effects of barrier thinning on small-signal and 30-GHz power characteristics of AlGaN/GaN heterostructure field-effect transistors," *IEEE Trans. Electron Devices*, vol. 58, no. 6, pp. 1681–1686, Jun. 2011, doi: 10.1109/TED.2011.2131653.

[24] Y.-K. Lin et al., "High-performance GaN MOSHEMTs fabricated with ALD Al_2O_3dielectric and NBE gate recess technology for high frequency power applications," *IEEE Electron Device Lett.*, vol. 38, no. 6, pp. 771–774, Jun. 2017, doi: 10.1109/LED.2017.2696569.

[25] F. Lecourt et al., "Power performance at 40 GHz on quaternary barrier InAlGaN/GaN HEMT," *IEEE Electron Device Lett.*, vol. 34, no. 8, pp. 978–980, Aug. 2013, doi: 10.1109/LED.2013.2266123.